Integration of Geometrically Different Elements to Design Thin Near-Field Metasurfaces

HAIDER ALI [1], (Member, IEEE), **MUHAMMAD U. AFZAL**[2], (Senior Member, IEEE), **KARU P. ESSELLE**[2], (Fellow, IEEE), AND **RAHEEL M. HASHMI**[1], (Member, IEEE)

[1] School of Engineering, Macquarie University, Sydney, NSW 2109, Australia
[2] School of Electrical and Data Engineering, University of Technology Sydney, Ultimo, NSW 2007, Australia

Corresponding author: Haider Ali (haider.ali@hdr.mq.edu.au)

ABSTRACT Phase-gradient metasurfaces, also known as phase-shifting surfaces, are used to steer the beam of medium-to-high gain antennas. Almost all such surfaces are made of cell elements that are similar in shape and only differ in dimensional parameters to achieve the required spatial phase gradient. A limitation of using the same geometry for the cell elements is that only limited phase shift range can be achieved while maintaining high transmission through each cell. A new strategy of integrating geometrically different cell elements, having different transmission phase and amplitude characteristics, is presented in this article. To demonstrate the concept, four different cell geometries are considered. The results indicate that the hybrid approach allows the designer to achieve the required phase shift range together with a high transmission with thinner metasurfaces having fewer dielectric and metal layers. When used to steer the beam of a microstrip patch array, the hybrid metasurface produced more accurate beam steering with 1.6° less steering error compared to a reference single-geometry metasurface.

INDEX TERMS Phase shifting surface, PSS, metasurface, beam steering, cell, metamaterial, hybrid, meta-steering, near field, phase transformation, beam scanning.

I. INTRODUCTION

Beam steering of an array antenna is a crucial area of research in microwave engineering. Several beam steering techniques exist, including mechanical and electronic steering [1]–[4]. The mechanical approach uses mechanical movement (tilting and rotation) of a reflector antenna or an antenna array to steer its beam. Mechanical tilting provides steering in elevation, and mechanical rotation provides steering in azimuth. Electronic steering is achieved by manipulating the excitation signals and the array geometry.

Mechanical tilting can cover a wide range of steering angles [5], [6]. They also do not contribute to the radiation losses of the base antenna. However, they are bulky and take a relatively larger physical space. Moreover, the mechanical tilting often requires heavy-duty motors, and they limit steering speed [3]. Electronic steering, on the other hand, is usually of low profile. It does not need mechanical movement, and the steering is achieved almost instantaneously by controlling the input excitations on the go [7]. However, electronic steering is expensive for high-gain antennas, and

the feed and phase-shifting networks can become complex and challenging. Moreover, the feed network can contribute to losses and reduce the overall radiation efficiency of the antenna or array, especially with a large number of elements at higher microwave and millimetre-wave bands.

Recently, new tilting-free methods have been developed to overcome the limitations of both mechanical and electronic steering [8]–[14]. One of the promising techniques is to use a pair of phase-shifting metasurfaces in the far field of a horn antenna [15] or a pair of near-field phase transforming metasurfaces in the near-field region of a base antenna [16]. Later is of greater interest due to its attractive feature of much lower overall height. The critical component of such a metasurface based beam-steering system is a pair of near-field metasurfaces. Such metasurfaces are designed to transform a given near-field phase distribution of a fixed base antenna to a linearly increasing phase profile to tilt the antenna beam at an offset angle; i.e. steering the beam in elevation without tilting the base antenna. Our focus, in this article, is on designing a new hybrid near-field metasurface using geometrically different cells. In the rest of the paper, we will refer to near-field phase transforming metasurfaces, interchangeably and simply, as metasurfaces for brevity.

A metasurface is essentially a flat and relatively thin sheet made up of small blocks called cells [15], [16]. Each cell consists of several dielectric and microstrip layers. The number of layers in a cell affects several parameters including maximum phase range the cell can achieve with high-transmission magnitude, losses, and bandwidth [16], [17]. A detailed study conducted for a cell in [17] concludes that the maximum phase range with high-transmission magnitude increases with the number of metal layers in the cell element. In this study, one-layered cells with transmission magnitude more than −3 dB can achieve a maximum phase range of 60°. The phase range increased to 180° and 300°, with cells having two and three metal layers, respectively. The complete phase range of 360° was achieved with a cell having four metal layers. The overall bandwidth of the printed cells is adversely affected by the number of layers, as increasing the number of layers corresponds to a higher-order band-pass filter. Increasing the order of a filter decreases its transition region and thus, the operating frequency band [17]–[19]. Almost all multilayered printed cell elements use dielectric layers in between adjacent metal layers. Therefore, increasing the number of layers contributes to ohmic and dielectric losses [17], [20].

In most of the studies conducted in the literature, only one type of geometry, for example, a square is considered for the patch layer. The authors then manipulate the patch dimensions, the number of layers, and the dielectric properties (dielectric constant, thickness etc.) to achieve their desired phase range with acceptable transmission amplitude. The limitation of such an approach, however, is the lack of complete (0° - 360°) phase range with a good transmission amplitude. To address this limitation, in all of the traditional metasurface-based designs, three to four layers are used to achieve the required phase range of 360° with sufficient transmission magnitude. Moreover, some phase shifts are not as exact as required, and the corresponding transmission is low. Less precise phase shifts lead to inaccurate steering, while low transmission amplitude introduces radiation losses due to reflections. Moreover, increasing the number of layers to achieve a larger phase shift range adds to the cost, thickness and weight of metasurfaces. In this article, we aim to achieve a more accurate transmission phase and amplitude with a hybrid approach by considering several different patch geometries. The number of layers and dielectric properties remain the same for all geometries.

This article is organized as follows. Section II reviews the configuration of the near-field metasurfaces. A new hybrid configuration of the metasurfaces will be discussed in Section III, followed by a hybrid design example with results in section IV. In section IV, we also compare the performance of the hybrid design to a reference metasurface made of square geometry only. The paper is concluded in section V.

II. BASICS OF METASURFACE MECHANISM
For the near-field metasurface to produce the desired beam tilt, its constituent cells should be able to have the required phase shift with acceptable transmission amplitude [16].

The near-field arrangement allows the metasurface to be physically placed very close to a base antenna. This makes the overall profile of the antenna including metasurface much smaller as opposed to a far-field metasurface where the surface has to be at a distance of several wavelengths from a horn antenna to make use of Geometric Optics approximations [15]. Low profile antennas are desirable for some applications such as on-the-move communication systems. We will now discuss the cell design in more details, followed by selected geometries for the hybrid metasurface design.
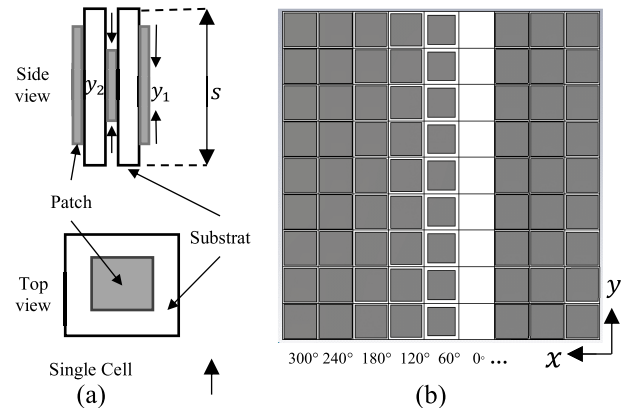

FIGURE 1. The metasurface design concept: (a) a cell's side and top view and (b) top view of a metasurface made up of cells. The grey colour represents conducting patch while the white colour represents the substrate.

A. CELL DESIGN
A cell element is the fundamental building block of any metasurface. Typically, each cell consists of dielectric and conductive layers. The conductive layer is usually a patch of a particular geometry. The patch geometry is optimized to obtain desired transmission properties (transmission amplitude and phase shift introduced by the cell) as per the application's requirements. Figure 1 depicts the concept of a cell and a metasurface with two dielectric layers and three microstrip layers. For simplicity, a square microstrip is shown. The top and bottom square patches have the same dimensions with a side length of y_1 while the middle patch has dimensions of $y_2 \times y_2$. The dielectric substrate dimensions are the same as the size of the cell, which is $s \times s$. The cell dimension s is chosen according to the design frequency and should be kept less than half the wavelength to avoid the onset of grating lobes and excessive discretization error [15], [16]. The substrate thickness is usually kept constant according to the bandwidth requirement and chosen as per the availability from the manufacturer. In all our design cases, the substrate was Rogers RT5880 of thickness 0.787 mm, selected due to its low dielectric constant (ϵ_r) of 2.2 and loss tangent ($tan\delta$) of 0.0009.

To observe its transmission properties, a cell is simulated for each possible dimension by varying its metallic patch size. For example, in the case of a square patch, the side length of the patch is varied from 0 mm to its maximum size which is

equal to the size of the cell. Each patch size will correspond to a specific phase shift with a particular transmission amplitude. This parametric simulation, also called a parametric sweep, will give us a set of data which we can analyse for further properties of the cell as will be discussed in detail in section III and IV.

B. DESIGN OF A METASURFACE OR PHASE SHIFTING SURFACE

To design a near-field metasurface, we use the basic array theory. To steer the beam of a linear array towards an elevation angle θ in spherical coordinates, the excitations of the individual array's elements must have a progressive phase shift where the phase shift increases linearly with a constant step or ϕ_e (in degrees), which is given by:

$$\phi_e = \frac{2\pi}{\lambda_0} d \sin \theta \qquad (1)$$

where λ_0 is the frequency of operation, and d is the inter-element spacing of the array.

Using the same approach, we design a linear phase progression (LPP) near-field phase-shifting metasurface that will steer an electromagnetic wave, after passing through it, towards an elevation angle θ. The individual cells will induce a phase shift to the incident wave. Cells are arranged such that the consecutive cells produce linear phase progression ϕ_e corresponding to the steering angle θ. The azimuth steering is achieved via rotating the surface manually along its axis. To achieve the full range of elevation and azimuth steering a second LPP metasurface is used [15], [16]. However, in this report, we are only focusing on the design and analysis of one metasurface. The concept can be extended to any relevant application.

A reference LPP metasurface is given in Figure 1 (b) made of square cells based on the design presented in [15]. This metasurface is designed to steer the incident wave towards an elevation angle of 28.8°, which according to (1), corresponds to a phase advance (ϕ_e) of 60° between adjacent columns. In the metasurface design, the cells are arranged such that the first column of the metasurface induces a phase delay of 300°; the second column generates a delay of 240° and so on. The simulation results for this metasurface will be given in section IV along with another hybrid metasurface for comparison. It is essential to mention that the specific phase delay is not significant. Rather the progressive phase difference between adjacent columns is critical, which in our case is 60°. Therefore, the first column of the metasurface can start with any phase value.

In the next section, we describe four different cell geometries that have been considered to design a hybrid metasurface.

III. SELECTED CELL GEOMETRIES

To demonstrate our concept of hybrid geometry of the near-field metasurfaces, we have considered four different cell geometries. These geometries are (i) Circular
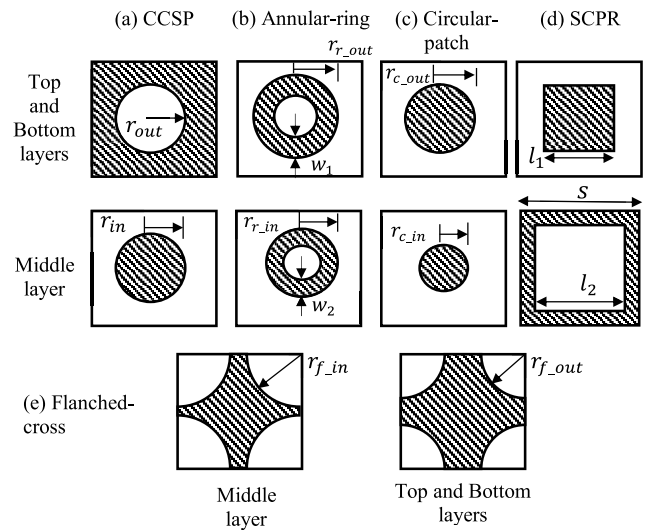

FIGURE 2. Cell geometries: (a) Circular Complementary Slots and Patch (CCSP), (b) Annular-ring, (c) Circular-patch, (d) Square Complementary Patches and Ring (SCPR) and (e) Flanched-cross.
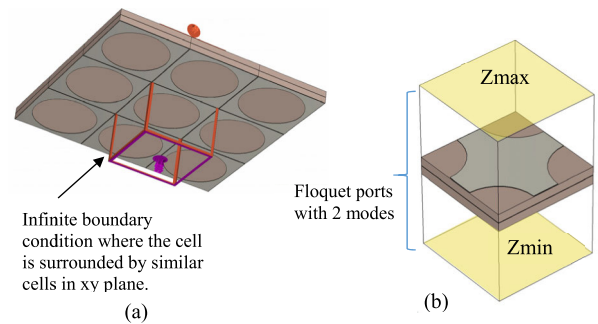

FIGURE 3. Simulation setup used for the analysis of cell elements. (a) Periodic boundary conditions in lateral directions to model infinitely extended metasurface in xy plane. (b) Input and output ports to excite the cell and observe transmission through the cell.

Complementary Slots and Patch (CCSP), (ii) Annular-ring, (iii) Circular-patch, (iv) Square Complementary Patches and Ring (SCPR), and (v) Flanched-cross. These geometries are shown in Figure 2 (a) – (e), respectively. In the following subsections, each of these geometries are described in detail.

A. CIRCULAR COMPLEMENTARY SLOTS AND PATCH (CCSP)

This geometry consists of a square patch on the top and bottom layers and has a circular slot of radius r_{out} at the centre, as shown in Figure 2 (a). The middle patch layer is a circle of radius r_{in}. The transmission through cells was characterised through Floquet mode analysis with CST Microwave Studio, using two de-embedded ports in the direction of field propagation. The cells were assigned periodic boundary conditions in the lateral directions and were excited with a plane wave through one of the two ports, as shown in Figure 3. This approach of designing near-field metasurfaces has been successfully demonstrated in previous

publications [16], [20]–[22] where sometimes metasurfaces are as close as a quarter of free-space wavelength to a base antenna. It is to be mentioned here that the plane wave excitation does not account for the mutual coupling between the actual base antenna and the metasurface. Such mutual coupling, however, is accounted for in the full-wave simulation setup where metasurface is placed within the near-field region of the base antenna, as described in section IV.
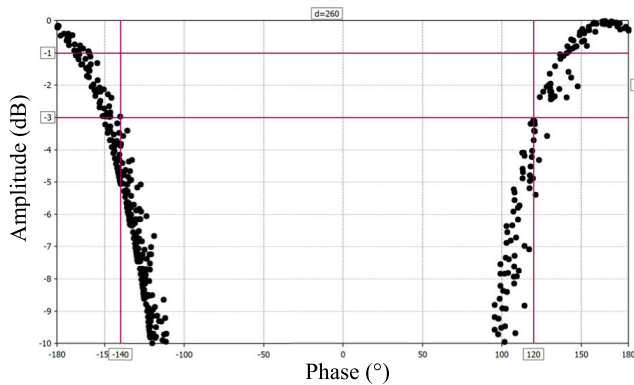

FIGURE 4. Transmission's phase vs amplitude plot for CCSP geometry.

The values of the two parameters r_{in} and r_{out} were varied across the range from 0.1mm to half the cell size ($s/2$) in steps of 0.1 mm, and the cell was simulated for each parametric value. The transmission amplitude (in dB) and phase shift (in degrees) of the cell were recorded for all parametric simulations. Figure 4 shows the phase vs amplitude plot that was drawn from the results of all the parametric studies. For brevity, only those parametric results have been shown which has an amplitude greater than -10 dB. Although Figure 4 does not show the values of r_{in} and r_{out}, the phase and amplitude values displayed correspond to the parametric values of r_{in} and r_{out}. The purple lines drawn in Figure 4 indicate the phase range where the magnitude is larger than -1 dB and -3 dB, respectively. As can be seen in Figure 4, the phase range that can be achieved with transmission >-3dB is from $120°$ to $180°$ and from $-140°$ to $-180°$ whereas for transmission >-1 dB the phase range is even shorter. This geometry can be useful to achieve phase shifts at the extremities of the $360°$ phase range.

Note that we are not using a circular slot in the middle layer of CCSP similar to its top and bottom layers. The reason is that when repeated in two dimensions, CCSP cells and flanched-cross cells lead to precisely the same double-infinite metasurface.

B. ANNULAR-RING

The annular-ring cell consists of rings on three metal layers. The top and bottom layers have the same radius (r_{r_out}) while the middle layer has a different radius (r_{r_in}). The width of the ring for the top/bottom layer is w_1 while that for the middle layer is w_2. As before, parametric sweeps were carried out for r_{r_out}, r_{r_in}, w_1, and w_2. The corresponding transmission
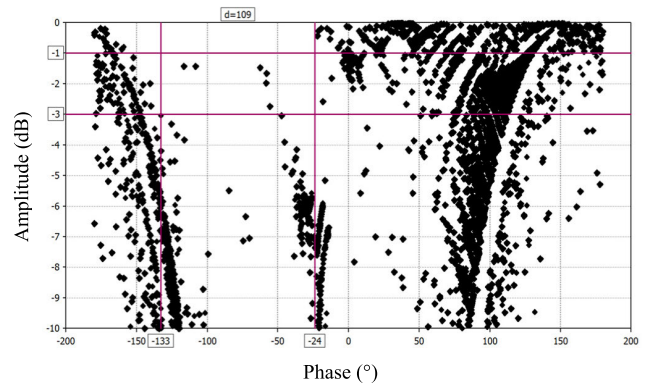

FIGURE 5. Transmission's phase vs amplitude plot for Annular-ring geometry.
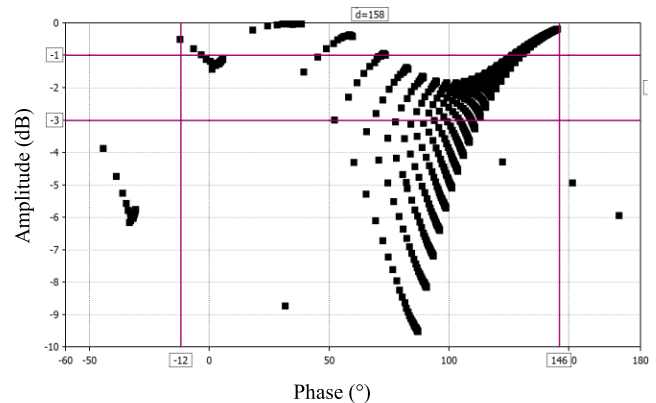

FIGURE 6. Transmission's phase vs amplitude plot for Circular-patch geometry.

amplitudes and phase shifts are shown in Figure 5. We see in Figure 5 that the entire phase range is covered with amplitude greater than -3 dB except for the subrange from $-133°$ to $-24°$ wherein some discrete phases (but not the whole subrange) are covered within -3 dB amplitude level.

C. CIRCULAR-PATCH
Similarly, the parametric sweeps were conducted for the circular-patch cell, which has circular patches on all three layers. Similar to previous cases, the top and bottom layers have the same dimensions with a radius of r_{c_out} while the middle layer has a different radius r_{c_in}. The resulting phase vs amplitude plot is given in Figure 6, which shows that the phase range covered with amplitude >-3dB is from $-12°$ to $146°$ and for amplitude >-1 dB it is from $-12°$ to $73°$ and from $125°$ to $145°$, respectively. It should be mentioned at this point that near-field metasurfaces require nearly all cells to have high transmission magnitude, preferably higher than -1dB. The plot in Figure 6 has been magnified to the area of interest (amplitude >-10 dB) for better visibility.

D. SQUARE COMPLEMENTARY PATCHES AND RING (SCPR)
The SCPR structure has squares patches on the top and bottom layers, whereas the middle layer has a square patch with
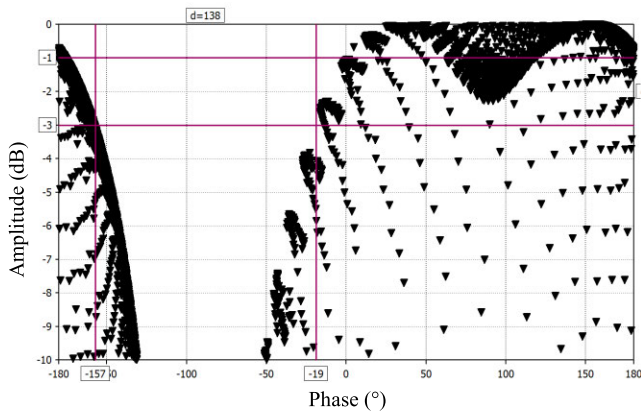
FIGURE 7. Transmission's phase vs amplitude plot for SCPR geometry.

FIGURE 8. Transmission's phase vs amplitude plot for flanched-cross geometry.

a square slot at its centre. Like previous cells, this cell has the same top and bottom layer patch sizes, which is different from the middle patch. The top and bottom squares have dimensions of $l_1 \times l_1$. The middle layer is a square patch of dimension $s \times s$ with a square slot of size $l_2 \times l_2$ at its centre. The width of one side of the square-strip is $s-l_2$. A parametric sweep is then performed for the parameters l_1 and l_2. The phase vs amplitude plot of the sweep is given in Figure 7. The phase ranges for transmission >-3dB are from $-180°$ to $-157°$ and from $-19°$ to $+180°$ while that for transmission >-1 dB are from $-180°$ to $-175°$ and from $-3°$ to $+180°$.

E. FLANCHED CROSS
The flanched cross cell is formed by cutting out a segment of a circle from each corner of a square patch. The centres of the circular patches are the corners of the square. It is essential to mention here the geometrical similarity of the flanched cross with that of CCSP. When flanched-cross geometry is repeated infinitely in two dimensions, its top and bottom layers resemble the CCSP geometry. However, the middle patch layers are different because, in the case of CCSP, the middle layer is a circle. In contrast, in the case of Flanched-cross, it is a flanched cross similar to top and bottom layers but with a different radius. Thus the infinite CCSP's middle layer consists of circular patches while that of Flanched-cross consists of circular slots.

The parametric sweeps were performed for the circles' radii for both inner (r_{f_in}) and outer (r_{f_out}) metal layers. The results of the parametric sweep are given in Figure 8 as a phase (in degrees) vs magnitude (in dB) plot. As it is evident from Figure 8, the entire phase shift range is achieved with transmission >-3 dB. However, a specific portion of the phase range is outside the range of transmission amplitude >-1 dB. It is worth mentioning that when the values of r_{f_in} or r_{f_out} are greater than half the size of the cell i.e. $r_{f\_in} > s/2$ or $r_{f_{out}} > s/2$ then the flanched cross shape reduces to a diamond shape.
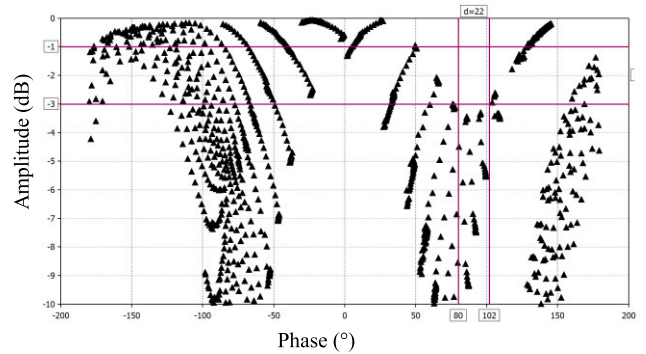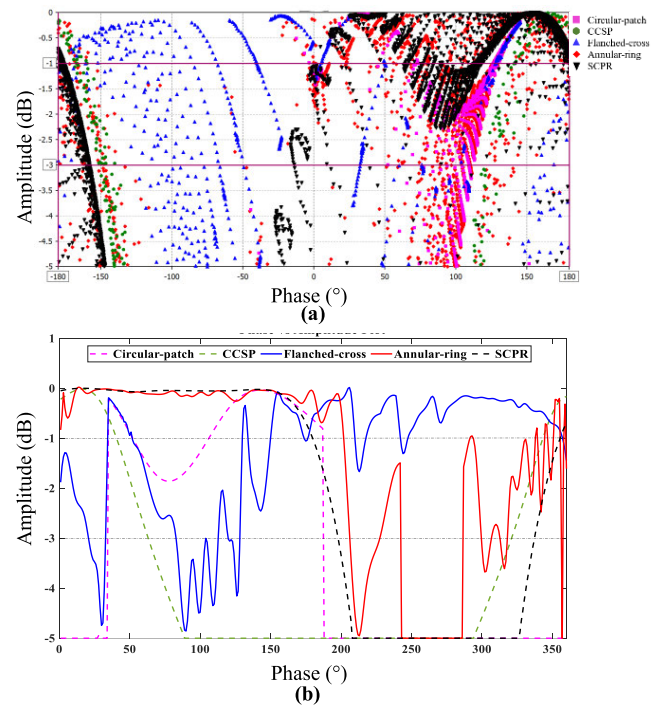

FIGURE 9. The phase vs amplitude plot showing the phase range that can be produced by a cell from four different geometries. (a) Discrete scatter plot, (b) a phase-normalized envelope curve plot showing the transmission behaviour of each geometry in the phase-amplitude domain.

IV. A HYBRID APPROACH TO ACHIEVE OPTIMIZED RESULTS
As was discussed in the introduction, in traditional metasurface design, only one type of geometry is considered for cell design. The limitation of such an approach is the lack of complete (0° - 360°) phase range with a good transmission amplitude. Therefore, to remedy this limitation, we examined various geometries in the previous section. Figure 9 shows the phase ranges that are covered by the four aforementioned cell geometries.

Figure 9(a) shows the actual discrete phase-amplitude values of the transmission of each geometry. Figure 9(b) shows

an envelope version of Figure 9(b) for ease of understanding of each geometry's transmission properties. The plot in Figure 9(b) is a normalized phase, which shows the phase range that can be produced by each geometry relative to other geometries. Almost the whole 360° phase range is covered with −1 dB or better transmission amplitude except for very few phases with slightly lower amplitude. This arrangement restricts the number of substrate layers to only two and that of metal layers to only three, putting an upper bound on the cost of the metasurface fabrication. Additionally, it also reduces the weight and thickness of the metasurface, which is desirable in specific applications that require low-profile antennas. Moreover, as mentioned previously, a lower number of layers means a larger bandwidth [17].
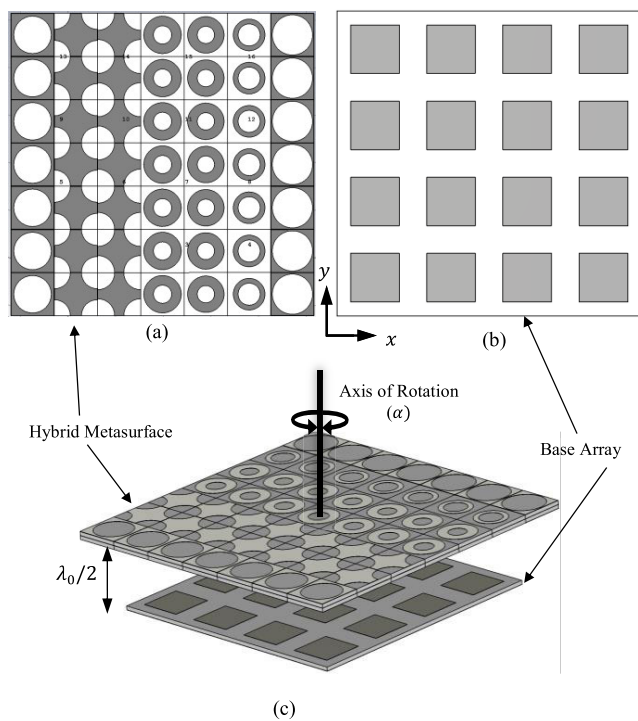

(a)

(b)

(c)

FIGURE 10. (a) Top view of hybrid metasurface made from cells of different geometries, (b) top view of a 4 × 4 microstrip patch array used as the base antenna with a fixed beam, and (c) a perspective view of the combined metasurface and the base antenna.

A. A HYBRID EXAMPLE

A near-field metasurface made of cells from different geometries is given in Figure 10(a). The metasurface was designed to steer the beam towards an elevation angle of 28.8°. The corresponding input progressive phase shift ϕ_e is 60°, as mentioned before. The individual cells required for different phase delays were selected by choosing a geometry that produces maximum transmission and minimum phase error for that particular value of the phase delay. Table 1 shows the parameter values of all the selected cells corresponding to the required phase delays, along with the transmission properties. For this particular metasurface design,

TABLE 1. Parameter values of the cells selected for the design of the hybrid metasurface.

Required Phase (°)	Geometry	Achievable Phase (°)	Phase Error (°)	Trans. Amplitude (dB)	Parameter Values (mm)
+/-180	CCSP	-179.7	0.3	-0.22	r_{out}: 3.9 r_{in}: 3.2
-120	Flanched-cross	-119.9	0.1	-0.18	r_{f_in}: 0.7, r_{f_out}: 3.3
-60	Flanched-cross	-60.4	0.4	-1.69	r_{f_in}: 1.5, r_{f_out}: 3.5
0	Annular-ring	0.35	0.35	-0.15	r_{r_in}: 1.2, w_2: 3 r_{r_out}: 1.9, w_1: 2
60	Annular-ring	60.2	0.2	-0.16	r_{r_in}: 0.5, w_2: 3 r_{r_out}: 1.8, w_1: 2
120	Annular-ring	120.2	0.2	-0.1	r_{r_in}: 2.5, w_2: 1 r_{r_out}: 2.3, w_1: 1

the optimal transmission properties were produced by the CCSP, flanched-cross and Annular-ring cell geometries.

The designed hybrid metasurface is then placed on top of a 4 × 4 microstrip array (shown in Figure 10(b)) at a distance of $\lambda_0/2$ from the array. A perspective view of the combined structure is given in Figure 10(c). The microstrip array with a fixed beam is used here as the base antenna for concept validation. Still, it can be replaced with any other type of base antenna as required. It is also important to mention here that individual patch elements of the microstrip array are fed on the vertical edges which cause them to produce a linear polarisation. More detail on the polarisation is given later.

The combined antenna system was simulated in CST Microwave Studio. The array's far-field directivity patterns before (black curves) and after combining with the hybrid metasurface (red curves) are shown in Figure 12. The array's main beam was successfully directed towards $\theta = 28.0°$ by the hybrid metasurface. As the target beam direction was 28.8°, there is a beam-steering error of 0.8° in all cases. This is due to: a. phase discretisation, b. slightly lower than desirable transmission in CCSP cells, and c. phase error due to lack of periodicity of the metasurface in the x-direction. Steering the beam in azimuth is achieved by rotating the metasurface. The angle of this rotation is denoted as α in Figure 12, which shows the antenna directivity pattern for $\alpha = 0°$, 90°, 180°, 270°.

The beam tilting of the combined structure is further demonstrated by plotting the electric field propagation in Figure 11 that is obtained from CST Microwave Studio simulations. Figure 11 (a) shows the timed snapshot of electric field propagation of the base microstrip patch array without the hybrid metasurface, which propagates and Figure 11 (b) shows the timed snapshot of electric field propagation with
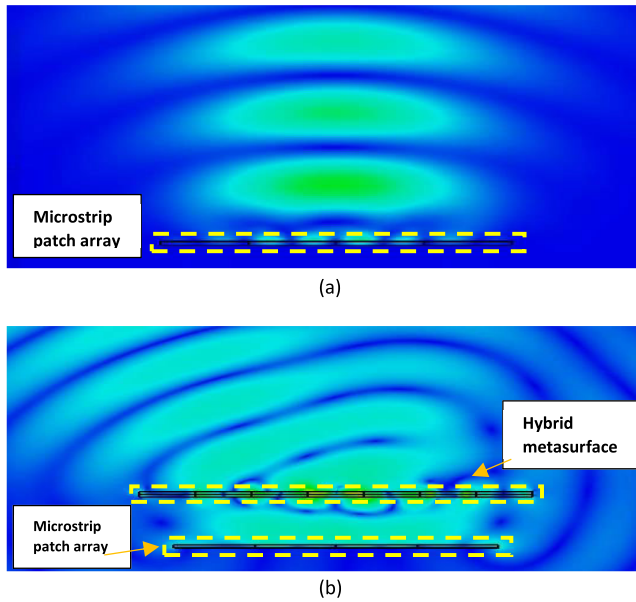
FIGURE 11. Snapshot of electric-field propagation in xz-plane for: (a) microstrip patch array only and (b) the combined structure of hybrid metasurface with array.

TABLE 2. Parameter values of the reference metasurface.

Desired Phase ϕ_e	y_1 (mm)	y_2 (mm)	Transmission Amplitude (dB)	Achievable Phase (°)	Phase Error (°)
±180	8	8.7	-10.3	-176.3	3.7
-120	7.8	8.7	-3.7	-122.2	2.2
-60	7.8	8.3	-0.3	-61.4	1.4
0	7.6	7.4	-1.2	-0.23	0.23
60	7.1	6.8	-0.5	59.9	0.1
120	4.9	4.1	-1.3	120.1	0.1

the hybrid metasurface. As can be seen in Figure 11 (b), with hybrid metasurface the direction of field propagation is at an angle away from the normal.

To compare the performance of the hybrid metasurface, a reference metasurface made of only one type of cells, i.e., square-patch geometry [15], was also designed and simulated with the same base antenna. Table 2 gives the cell dimensions of the reference metasurface to achieve steering for $\theta = 28.8°$ where y_1 and y_2 are, respectively, the side lengths of square patches for the top/bottom and middle layers. The thickness, material, and other properties of the substrate and metal layers were kept exactly the same as those of the hybrid metasurface for coherency. The far-field directivity patterns of the array when steering with the reference metasurface is also given in Figure 12 (blue curves). We see in Figure 12 that the beam steering error is 2.2° when using the reference metasurface.

The increased error in this case, as compared to the hybrid case, is possibly due to the decreased transmission amplitude and increased phase error of the individual reference cells, which are given in Table 2. The worst phase error in the case of the hybrid metasurface is 0.4° while in the case of the
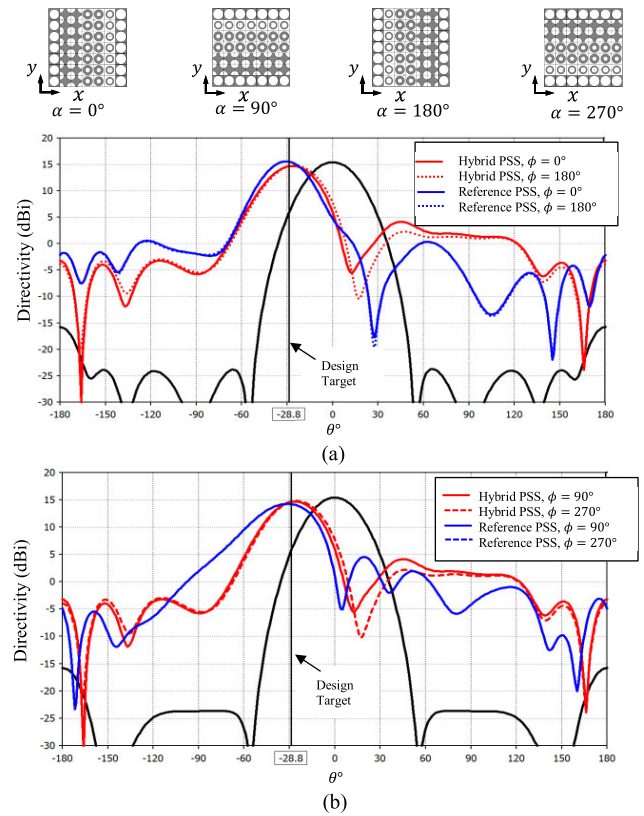

FIGURE 12. Directivity pattern of the 4 × 4 array when its beam is steered towards $\theta = 28.8°$, (a):$\phi = 0°$, 180° and (b):$\phi = 90°$, and 270° with the hybrid metasurface (red) and the reference square-patch metasurface (blue).

reference metasurface it is 3.7°. Likewise, the worst transmission amplitude for the hybrid metasurface is −1.69 dB while that for the reference metasurface is −10.3 dB.

The directivity of the base-antenna array without a metasurface is 15.4 dBi. It was slightly reduced by the hybrid metasurface to 14.7 dBi for $\phi = 0°$, 180° and 14.8 dBi for $\phi = 90°$, 270°. Comparatively, the reference metasurface did not affect the array's directivity for $\phi = 0°$, 180°; however, it did reduce the directivity to 14.2 dBi in the case of $\phi = 90°$ and 270°. Moreover, the sidelobe level (SLL) of the radiation pattern is slightly higher for $\phi = 90°$, 270° in comparison to $\phi = 0°$, 180° for the reference metasurface. It is interesting to note that both the hybrid and reference metasurface increased the SLL of the beam. Unless extensive optimisations are done to reduce sidelobes and grating lobes, sidelobes of this level are common in beam-steering antenna systems based on metasurfaces [23].

We also investigated the polarization of the antenna with and without metasurface in the far-field region. The two polar components E_θ and E_ϕ of the antenna array, without metasurface, at azimuth angles $\phi = 0°$ and $\phi = 90°$ are plotted in Figure 13. The co- and cross-polar components at azimuth angle $\phi = 0°$ is E_θ and E_ϕ, respectively. Since all cells
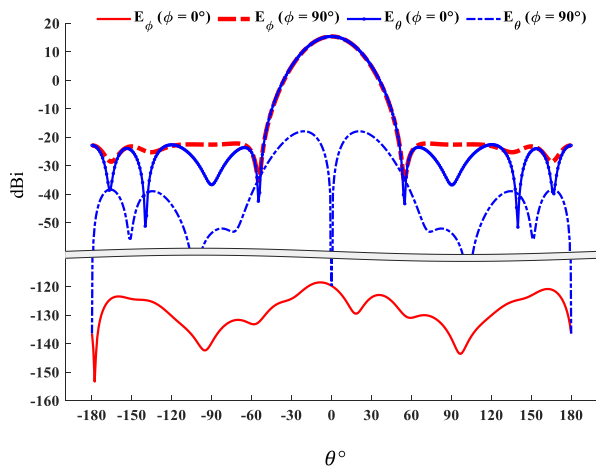
FIGURE 13. The polarisation of the base microstrip array at 11.5 GHz for azimuth angles: $\phi = 0°$ and $90°$. The main beams of E_θ, $\phi = 0°$ and E_ϕ, $\phi = 90°$ are overlapping.
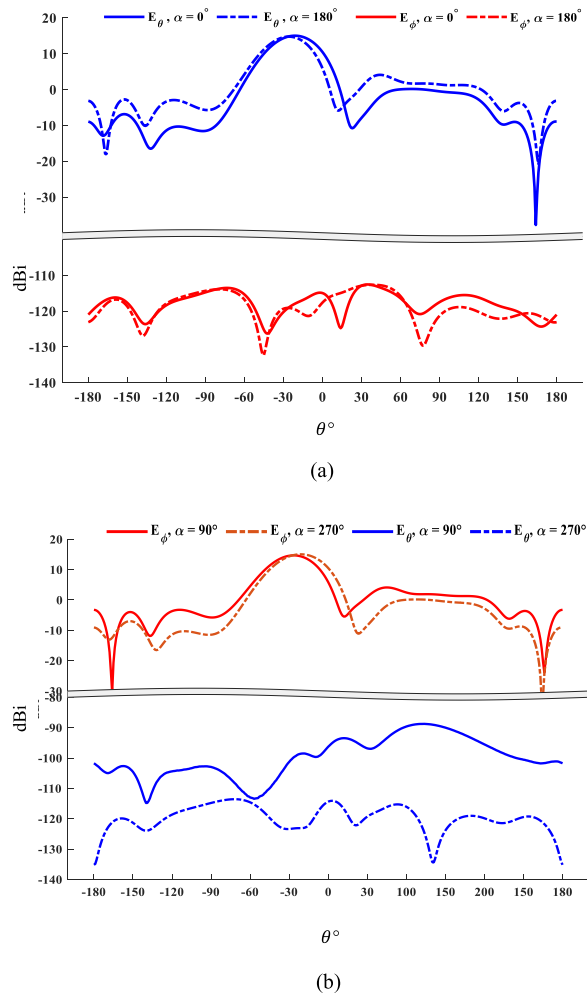

(a)

(b)

FIGURE 14. The polarisation of the radiated field with E_θ and E_ϕ components for (a) $\alpha = 0°$, $180°$ and (b) $\alpha = 90°$, $270°$.

used in the hybrid metasurface have 90° rotational symmetry, the metasurface is not expected to alter the polarization of the antenna array. To confirm this, we have also plotted the two

(a) $\alpha = 0°$

(b) $\alpha = 90°$

(c) $\alpha = 180°$
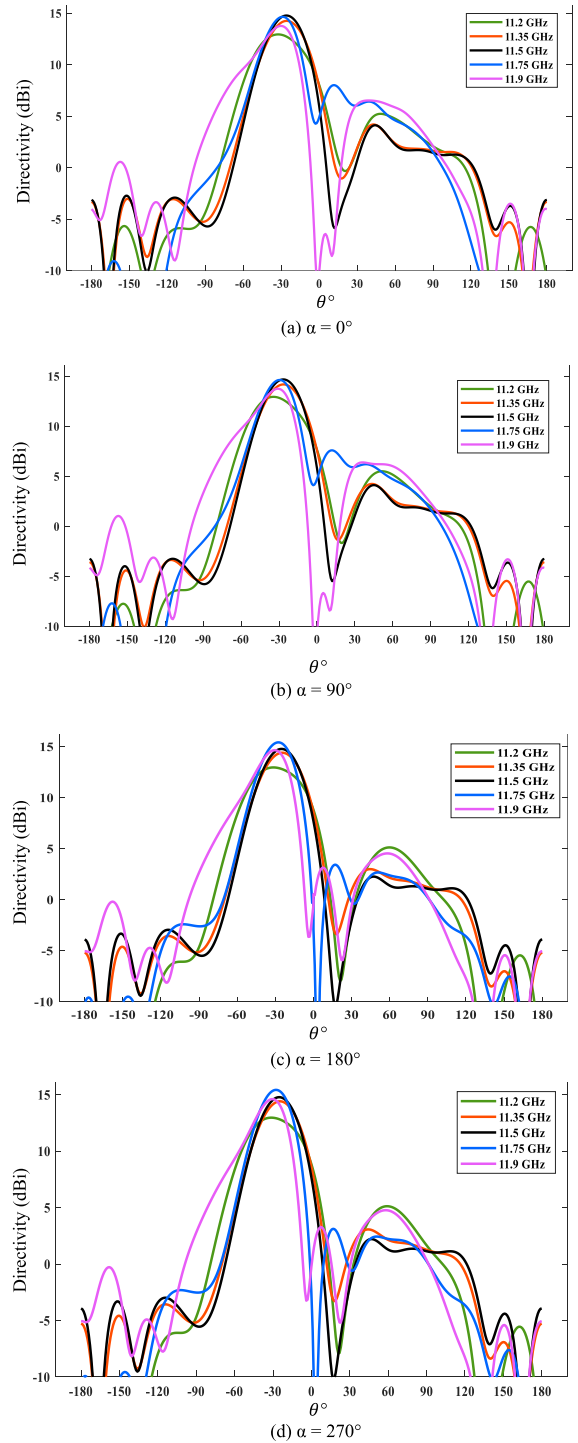
(d) $\alpha = 270°$

FIGURE 15. Far-field directivity patterns of the combined structure of metasurface and microstrip array for $\alpha = 0°$, $90°$, $180°$, and $270°$.

polar components of the array with metasurface in Figure 14. These pattern cuts are taken at the azimuth angles containing the beam peaks for the four rotation angles of the metasurface $\alpha = 0°$, $90°$, $180°$, and $270°$. As an example, for rotation angles $\alpha = 0°$ and $180°$, the beam peak is at azimuth angles $\phi = 0°$ and $180°$, respectively. As shown in Figure 14 (a), at these azimuth angles, the co-polar component is E_θ.

When beam peak is at azimuth angles $\phi = 90°$ and $270°$ for the metasurface rotation angles $= 90°, 270°$, in Figure 14(b), the co-polar component is E_ϕ. The axial-ratio (AR) in the main beam direction for all cases of metasurface rotation is more than 34 dB, which confirms the linear polarization of the array with the metasurface.

We simulated the metasurface with the array in a frequency band between 10 GHz and 13 GHz for the four metasurface rotation angles $\alpha = 0°, 90°, 180°,$ and $270°$. The 3 dB directivity band of the system, when calculated using directivity values in a fixed direction, is between 11 GHz and 12 GHz with a directivity bandwidth of 1GHz. The directivity pattern cuts taken at five frequencies in the band are plotted in Figure 15. The antenna system reasonably maintains the pattern quality throughout the band.

From the results given in Figure 12 and aforementioned discussion, it is evident that the hybrid approach towards the metasurface design for beam steering application has advantages when it comes to achieving the full 360° phase range with high transmission amplitude and a minimal number of substrate layers.

V. CONCLUSION
The traditional approach to design a phase-shifting surface for antenna beam steering is to use a single cell geometry while playing with the dimensions and the number of the dielectric and conducting layers. However, one cell geometry is not enough to achieve the full 360° phase range with good transmission amplitude (>-3 dB for far-field metasurfaces and >-1 dB for near-field metasurfaces). This results in the need to increase the number of substrate and metal layers, thereby increasing the cost and weight of the antenna system. Thus, a hybrid geometry approach was explored in this article as a potential solution, with the focus on achieving optimal transmission magnitude and complete 360° phase range. It is shown, with an example metasurface design and verified with simulation results, that using multiple cell geometries, good transmission properties can be achieved with less number of layers. Such an approach provides better steering results with lower beam-steering error as compared to the traditional single-geometry approach. Moreover, the reduced number of layers contribute to the overall profile reduction of the antenna system and the cost of material and fabrication.

ACKNOWLEDGMENT

REFERENCES
[1] I. Uchendu and J. R. Kelly, "Survey of beam steering techniques available for millimeter wave applications," *Prog. Electromagn. Res. B*, vol. 68, pp. 35–54, 2016, doi: 10.2528/PIERB16030703.

[2] C. A. Balanis, *Antenna Theory: Analysis and Design*. Hoboken, NJ, USA: Wiley, 2016.

[3] S. Borisov and A. Shishlov, "Antennas for Satcom-on-the-move, review," in *Proc. Int. Conf. Eng. Telecommun.*, Moscow, Russia, Nov. 2014, pp. 3–7.

[4] A. A. Baba, R. M. Hashmi, K. P. Esselle, M. Attygalle, and D. Borg, "A millimeter-wave antenna system for wideband 2-D beam steering," *IEEE Trans. Antennas Propag.*, vol. 68, no. 5, pp. 3453–3464, May 2020.

[5] K. W. Linnes, W. D. Merrick, and R. Stevens, "Ground antenna for space communication system," *IRE Trans. Space Electron. Telemetry*, vol. SET-6, no. 1, pp. 45–54, 1960.

[6] E. Phillips and P. J. B. Clarricoats, "Optimum design of a Gregorian-corrected spherical-reflector antenna," in *Proc. Inst. Elect. Eng.*, Apr. 1970, vol. 117, no. 4, pp. 718–734.

[7] H. J. Visser, *Array and Phased Array Antenna Basics*. Hoboken, NJ, USA: Wiley, 2005.

[8] K. P. Esselle, "A brief overview of antenna technologies for communications-on-the-move satellite communication mobile terminals," in *Proc. IEEE Antennas Propag. Soc. Int. Symp.*, Montreal, QC, Canada, 2020.

[9] K. P. Esselle, "Mobile satellite communication terminals—State of the art and antenna challenges," in *Proc. 14th Eur. Conf. Antennas Propag.*, Copenhagen, Denmark, 2020.

[10] Y.-B. Jung, S.-Y. Eom, S.-I. Jeon, A. V. Shishlov, and C.-J. Kim, "Novel hybrid antenna design having a shaped reflector for mobile satellite communication applications," in *Proc. IEEE Antennas Propag. Soc. Int. Symp.*, Toronto, ON, Canada, Jul. 2010, pp. 1–4.

[11] Y.-B. Jung, A. V. Shishlov, and S.-O. Park, "Cassegrain antenna with hybrid beam steering scheme for mobile satellite communications," *IEEE Trans. Antennas Propag.*, vol. 57, no. 5, pp. 1367–1372, May 2009.

[12] Y. Yuan, K. Zhang, B. Ratni, Q. Song, X. Ding, Q. Wu, S. N. Burokur, and P. Genevet, "Independent phase modulation for quadruplex polarization channels enabled by chirality-assisted geometric-phase metasurfaces," *Nature Commun.*, vol. 11, no. 1, p. 4186, Dec. 2020.

[13] Y. Yuan, S. Sun, Y. Chen, K. Zhang, X. Ding, B. Ratni, Q. Wu, S. N. Burokur, and C. Qiu, "A fully phase-modulated metasurface as an energy-controllable circular polarization router," *Adv. Sci.*, vol. 7, no. 18, Sep. 2020, Art. no. 2001437.

[14] K. Zhang, Y. Yuan, X. Ding, B. Ratni, S. N. Burokur, and Q. Wu, "High-efficiency metalenses with switchable functionalities in microwave region," *ACS Appl. Mater. Interfaces*, vol. 11, no. 31, pp. 28423–28430, Aug. 2019.

[15] N. Gagnon and A. Petosa, "Using rotatable planar phase shifting surfaces to steer a high-gain beam," *IEEE Trans. Antennas Propag.*, vol. 61, no. 6, pp. 3086–3092, Jun. 2013.

[16] M. U. Afzal and K. P. Esselle, "Steering the beam of medium-to-high gain antennas using near-field phase transformation," *IEEE Trans. Antennas Propag.*, vol. 65, no. 4, pp. 1680–1690, Apr. 2017.

[17] N. Gagnon, "Phase shifting surface (PSS) and phase and amplitude shifting surface (PASS) for microwave applications," Ph.D. dissertation, Fac. Eng., Univ. Ottawa, Ottawa, ON, Canada, 2011.

[18] C. Saeidi and D. V. D. Weide, "Wideband plasmonic focusing metasurfaces," *Appl. Phys. Lett.*, vol. 105, no. 5, Aug. 2014, Art. no. 053107.

[19] A. A. Fathnan and D. A. Powell, "Bandwidth and size limits of achromatic printed-circuit metasurfaces," *Opt. Exp.*, vol. 26, no. 22, pp. 29440–29450, Oct. 2018.

[20] A. E. Olk and D. A. Powell, "Accurate metasurface synthesis incorporating near-field coupling effects," *Phys. Rev. A, Gen. Phys.*, vol. 11, no. 6, Jun. 2019, Art. no. 064007.

[21] X. Zhao, C. Yuan, L. Liu, S. Peng, Q. Zhang, L. Yu, and Y. Sun, "All-metal beam steering lens antenna for high power microwave applications," *IEEE Trans. Antennas Propag.*, vol. 65, no. 12, pp. 7340–7344, Dec. 2017.

[22] F. Han and P. Liu, "Terahertz near-field metasurfaces: Amplitude–phase combined steering and electromagnetostatic dual-field superfocusing," *Adv. Opt. Mater.*, vol. 8, no. 6, Mar. 2020, Art. no. 1901331.

[23] K. Singh, M. U. Afzal, M. Kovaleva, and K. P. Esselle, "Controlling the most significant grating lobes in two-dimensional beam-steering systems with phase-gradient metasurfaces," *IEEE Trans. Antennas Propag.*, vol. 68, no. 3, pp. 1389–1401, Mar. 2020.

[24] H. Fernández Álvarez, M. E. de Cos Gómez, and F. Las-Heras Andrés, "On the broadening of single-layer metasurface bandwidth by coupling resonances," *Materials*, vol. 13, no. 9, p. 2063, Apr. 2020.

[25] H.-M. Lee and H.-S. Lee, "A method for extending the bandwidth of metamaterial absorber," *Int. J. Antennas Propag.*, vol. 2012, Jan. 2012, Art. no. 859429.

[26] X. Gao, L. Singh, W. Yang, J. Zheng, H. Li, and W. Zhang, "Bandwidth broadening of a linear polarization converter by near-field metasurface coupling," *Sci. Rep.*, vol. 7, no. 1, pp. 1–8, Dec. 2017.

HAIDER ALI (Member, IEEE) received the bachelor's degree in telecommunication engineering from the NWFP University of Engineering and Technology, Pakistan, and the master's degree in electrical engineering with an emphasis on signal processing from the King Fahd University of Petroleum and Minerals (KFUPM), Dhahran, Saudi Arabia, in 2012. He is currently pursuing the Ph.D. degree with the School of Engineering, Macquarie University, Sydney.

He was the Project Engineer of the Centre for Engineering Research, KFUPM. While in KFUPM, he has worked on several applied research projects. He was a Team Member with the Calibration and Metrology Laboratory, KFUPM, where he contributed to automating the calibration systems and improving their accuracy for electronic measuring instruments. His current research interests include developing flat-panel antennas for satellite-on-the-move communication systems and, specifically, finding new ways to improve existing antenna beam steering mechanisms using metamaterial.

MUHAMMAD U. AFZAL (Senior Member, IEEE) received the bachelor's degree (Hons.) in electronics engineering and the master's degree in computational science and engineering from the National University of Sciences and Technology (NUST), Islamabad, Pakistan, in 2005 and 2011, respectively, and the Ph.D. degree from Macquarie University, Sydney, Australia, in 2017.

He was a Lab Engineer with the Samar Mubarakmand Research Institute of Microwave and Millimeterwave Studies (SMRIMMS), Islamabad, from 2010 to 2012. He was a Lecturer with the Electrical Engineering Department, NUST, from 2012 to 2013. He developed the concept of near-field phase correction to enhance the directivity of low-gain aperture antennas in IEEE TAP paper titled "Dielectric Phase-Correcting Structures for Electromagnetic Band-Gap Resonator Antennas." His research interests include the development of electromagnetic phase-shifting structures, frequency selective surfaces, and similar metamaterials for microwave and millimetre-wave antenna applications. He is the Co-Inventor of efficient antenna beam-steering technology that has been developed using near-field metasurfaces, which received the Highly Commended Certificate in Five Future-Shaping Research Priorities category of 2017 Academic Staff Awards. He also led a Team of colleagues in a CSIRO sponsored ON Prime 2, in 2017–a pre-accelerator program designed to commercialize outcomes of academic research. He has received several awards and scholarships, including the Merit-Based Scholarship in six out of eight semesters during undergraduate, the Scholarship of Complete Fee Waiver during postgraduate studies, and the International Macquarie Research Excellence (iMQRES) Scholarship for his Ph.D. study from Macquarie University. He received the Competitive Travel Grant to present his research work at a Flagship Conference under the Antennas and Propagation Society (APS) in Vancouver, Canada, in 2015.

KARU P. ESSELLE (Fellow, IEEE) received the B.Sc. degree (Hons.) in electronic and telecommunication engineering from the University of Moratuwa, Sri Lanka, and the M.A.Sc. and Ph.D. degrees with near-perfect GPA in electrical engineering from the University of Ottawa, Canada.

He was the Director of the WiMed Research Centre and the Associate Dean–Higher Degree Research (HDR) of the Division of Information and Communication Sciences and directed the Centre for Collaboration in Electromagnetic and Antenna Engineering, Macquarie University, Sydney. He is currently the Distinguished Professor in electromagnetic and antenna engineering with the University of Technology Sydney and a Visiting Professor with Macquarie University. According to 2019 Special Report on Research published by The Australian National Newspaper, he is the National Research Field Leader in Australia in microelectronics and electromagnetisms fields. He has also served as a member of the Dean's Advisory Council and the Division Executive and the Head of the Department several times. He has authored approximately 600 research publications and his papers have been cited more than 10 000 times. In 2019, his publications received 1200 citations. He is the first Australian Antenna Researcher ever to reach Google Scholar H-index of 30 and his citation indices have been among the top Australian antenna researchers for a long time (at present: i10 is 182 and H-index is 49). His research has been supported by many national and international organizations, including the Australian Research Council, Intel, U.S. Air Force, Cisco Systems, Hewlett-Packard, the Australian Department of Defence, the Australian Department of Industry, and German and Indian governments.

Prof. Esselle is a Fellow of the Royal Society of New South Wales and Engineers Australia. After two stages in the selection process, he was also selected by this Society as one of two candidates in the ballot for the 2019 President of the Society. Only three people from Asia or Pacific apparently have received this honor in the 68-year history of this Society. He is also one of the three Distinguished Lecturers (DL) selected by the Society in 2016. He is the only Australian to Chair the Antennas and Propagation (AP) DL Program ever, the only Australian AP DL in almost two decades, and second Australian AP DL ever (after UTS Distinguished Visiting Professor Trevor Bird). He has been continuously serving as the IEEE AP Society Administrative Committee in several elected or ex-officio positions since 2015. Since 2002, his research team has been involved with research grants, contracts, and Ph.D. scholarships worth about 20 million dollars, including 15 Australian Research Council grants, without counting the 245 million-dollar SmartSat Corporative Research Centre, which started in 2019. His awards include one of the two finalists for 2020 Australian Eureka Prize for Outstanding Mentor of Young Researchers, the 2019 Motohisa Kanda Award (from IEEE USA) for the most cited paper in IEEE Transactions on Electromagnetic Compatibility in the past five years, the 2019 Macquarie University Research Excellence Award for Innovative Technologies, the 2019 ARC Discovery International Award, the 2017 Excellence in Research Award from the Faculty of Science and Engineering, the 2017 Engineering Excellence Award for Best Innovation, the 2017 Highly Commended Research Excellence Award from Macquarie University, the 2017 Certificate of Recognition from IEEE Region 10, the 2016 and 2012 Engineering Excellence Awards for Best Published Paper from IESL NSW Chapter, the 2011 Outstanding Branch Counsellor Award from IEEE headquarters, USA, the 2009 Vice Chancellor's Award for Excellence in Higher Degree Research Supervision, and the 2004 Innovation Award for best invention disclosure. His mentees have been awarded many fellowships, awards, and prizes for their research achievements. Theses of his Ph.D. graduates were examined by 53 international experts, who ranked them in the top 5% or 10%. Two of his recent students were awarded the Ph.D. degree with the highest honor at Macquarie University–the Vice Chancellor's Commendation. He has provided expert assistance to more than a dozen companies, including Intel, Hewlett Packard Laboratory, USA, Cisco Systems, USA, Audacy, USA, Cochlear, Optus, ResMed, and Katherine-Werke, Germany. His team designed the high-gain antenna system for the world's first entirely *Ka*-band CubeSat made by Audacy, USA, and launched to space by SpaceX, in December 2018. This is believed to be the first Australian-designed high-gain antenna system launched to space, since CSIRO-designed antennas in Australia's own FedSat launched in 2002. He is also in the College of Expert Reviewers of the European Science Foundation, for the period 2019–2022, and he has been invited to serve as an International Expert/Research Grant Assessor by several other research funding bodies as well, including the European Research Council and funding agencies in Norway, Belgium, The Netherlands, Canada, Finland, Hong Kong, Georgia, South Africa, and Chile. He has been invited by Vice-Chancellors of Australian and overseas universities to assess applications for promotion to professorial levels. He has also been invited to assess grant applications submitted to Australia's most prestigious schemes, such as Australian Federation Fellowships and Australian Laureate Fellowships. In addition to the large number of invited conference speeches he has given, he has been an invited plenary/extended/keynote speaker of several IEEE and other conferences and workshops, including EuCAP 2020 Copenhagen, Denmark; URSI 2019 Seville, Spain; and 23rd ICECOM 2019, Dubrovnik, Croatia. Since 2018, he has been the Chair of the prestigious Distinguished Lecturer Program Committee of the IEEE

AP Society–the premier global learned society dedicated for antennas and propagation, which has close to 10 000 members worldwide. He is also the Chair of the Board of management of Australian Antenna Measurement Facility. He was the elected Chair of IEEE New South Wales (NSW) and IEEE NSW AP/MTT Chapter, in 2016 and 2017. He is also the Track Chair of IEEE AP-S 2020 Montreal; the Technical Program Committee Co-Chair of ISAP 2015, APMC 2011, and TENCON 2013; and the Publicity Chair of ICEAA/IEEE APWC 2016, IWAT 2014, and APMC 2000. He is an Associate Editor of IEEE Transactions on Antennas and Propagation, *IEEE Antennas and Propagation Magazine*, and IEEE Access. His research activities are posted in http://web.science.mq.edu.au/~esselle/ and https://www.uts.edu.au/staff/karu.esselle.

RAHEEL M. HASHMI (Member, IEEE) received the B.S. degree (Hons.) from CIIT, Pakistan, the M.S. degree from the Politecnico di Milano, Italy, and the Ph.D. degree from Macquarie University, Australia.

He is currently a Senior Lecturer with the Faculty of Science and Engineering, Macquarie University. His research interests include novel antenna technologies and microwave/millimeter-wave devices for applications in communications sector, defense, and smart living. His research explores the electromagnetic response of artificially engineered materials, using them to manipulate electromagnetic radiation for creating simple, yet highly efficient antennas and wireless components. He has received more than 1.6 million dollars worth of research grants, contracts, and fellowships. He has contributed more than 80 peer-reviewed journal and conference papers, two scholarly book chapters, and is an inventor on two patent applications. From 2012 to 2015, he was a Visiting Researcher with the CSIRO Astronomy and Space Science Division, Australia. He was a recipient of several prestigious awards and fellowships, including the 2017 Young Scientist Award (Field and Waves) from the International Union of Radio Science (URSI), the 2012 Commonwealth IPRS Award, the CSIRO OCE Ph.D. Fellowship, and the Institute's Gold Medal from the CIIT, Pakistan. He was the Chair of the IEEE Antennas and Propagation/Microwave Theory and Techniques Joint Chapter from 2018 to 2019 and the Vice Chair of the IEEE Young Professionals Affinity Group in New South Wales from 2017 to 2018. He regularly reviews for several esteemed journals and conferences in his field, including the IEEE Transactions on Antennas and Propagation, the IEEE Antennas and Wireless Propagation Letters, IEEE Access, Asia–Pacific Microwave Conference, the International Conference on Electromagnetics in Advanced Applications, AP-S Symposium, and EuCAP. He serves as an Associate Editor for the *IET Microwaves, Antennas and Propagation*, and as a Guest Editor for IEEE Access and *Microwave and Optical Technology Letters* (Wiley).

• • •